Available online at www.sciencedirect.com

ScienceDirect

Energy Procedia 157 (2019) 1253–1265

Energy Procedia

www.elsevier.com/locate/procedia

Technologies and Materials for Renewable Energy, Environment and Sustainability, TMREES18, 19–21 September 2018, Athens, Greece

Decentralized Hamiltonian Control of Multi-DER Isolated Microgrids with Meshed Topology

Mohamed Toub[a,*], Rush D. Robinett III[b], Mohamed Maaroufi[a], Ghassane Aniba[a]

[a]*Mohammadia School of Engineering, Mohammed V University of Rabat, Rabat, Morocco*

[b]*Michigan Technological University, Houghton, MI, USA*

Abstract

The new electricity grid of the future, smart grid, can be seen as the interconnection of multiple microgrids. These microgrids are usually composed of distributed energy resources (DERs) that connect to each other in different topologies. Therefore, the modeling and control of meshed microgrids are requisite. This paper presents a mathematical approach for the modeling and decentralized control of multi-DER isolated microgrids (ImGs) with a meshed topology. Based on the advanced control scheme: Hamiltonian surface shaping and power flow control (HSSPFC), decentralized controllers are designed independently using only local information. These controllers regulate the voltage at the point of common coupling (PCC) of their respective DERs and guarantee the stability of the overall ImG without requiring any communication infrastructure; hence, avoiding a single point of failure and harvesting the scalability of the ImG.

Keywords: Decentralized control, distributed power generation, droop control, meshed topology, microgrids.

* Corresponding author. Tel.: +212-638-869-831.
E-mail address: mohamedtoub@research.emi.ac.ma

1876-6102
10.1016/j.egypro.2018.11.291

1. Introduction

The control strategies for microgrids are categorized into three hierarchical control levels: primary control, secondary control, and tertiary control [1]. The primary control ensures the system's reliability and resiliency since it does not rely on communication infrastructure and uses local controllers with fast response to ensure the system stability. The secondary control uses a central controller with relatively slower dynamics to restore the voltage and frequency and compensate the deviation caused by the primary control. Tertiary control adds an extra layer to ensure that the microgrid operates optimally and economically in the longer timescale.

Various control methods have been proposed in the literature for the primary control level. These methods can be categorized into two groups [2]. The first group includes the active load sharing methods such as the centralized method [3], the master-slave method [4], and the average load sharing method [5]. All these methods rely on communication infrastructure for measurements, supervision, and coordination of the distributed energy resources (DERs). The communication failure represents a single point of failure that jeopardizes the entire microgrid and can lead to its collapse. The second group includes the droop methods that only use local measurements to share the load and maintain the voltage without requiring any communication infrastructure [6].

Many research works that address the advanced control techniques for microgrids have been reported in the literature [7–10]. However, as reviewed in reference [11], the decentralized control of meshed microgrids has not been investigated significantly and remains an open research topic. The most important contribution in this area is the work of reference [12] that proposed a novel control scheme for islanded microgrids with meshed topology. In this work, decentralized controllers were designed to guarantee the stability of the overall isolated microgrid (ImGs) while regulating the voltage and frequency at the point of common coupling (PCC) of each DER. However, this design procedure cannot be considered completely decentralized since two global scalar quantities were used for the design of the controllers.

In this paper, a fully decentralized control scheme for multi-DERs ImGs with a meshed topology is presented. First, the state-space model of two interconnected DERs was developed. Next, the resulting state-space model was extended to ImGs with N interconnected DERs in a meshed topology. This model was then used to design the decentralized controllers based on the advanced design technique: Hamiltonian surface shaping and power flow control (HSSPFC) [13–17], which is a two-step analysis and design method for control laws [18]. The first step consists of shaping the Hamiltonian energy surface, using the integral gain of the controller, to guarantee the static stability. The second step is the power flow control that guarantees dynamical stability by choosing the proportional gain of the controller. This procedure allowed us to synthesize decentralized controllers that regulate the voltage at the PCC of their respective DERs and guarantee the stability of the overall ImG in a decentralized fashion, relying only on local information, and without requiring communication between DERs.

The rest of this paper is organized as follows. In Section 2, the state-space models of the subsystems and the meshed ImG are derived. Section 3 details the HSSPFC control design procedure and proves the stability of the ImG. Section 4 supports the design procedure with simulation and investigates the performance of the designed decentralized controllers. Section 5 concludes the paper.

2. Microgrid Model

2.1. Model of two interconnected subsystems

In this section, the state-space model of the studied ImG is developed. For simplification, the state-space equations of an ImG with two parallel subsystems denoted i and j are derived, then the resulting model is extended to ImGs with N subsystems in a meshed topology.

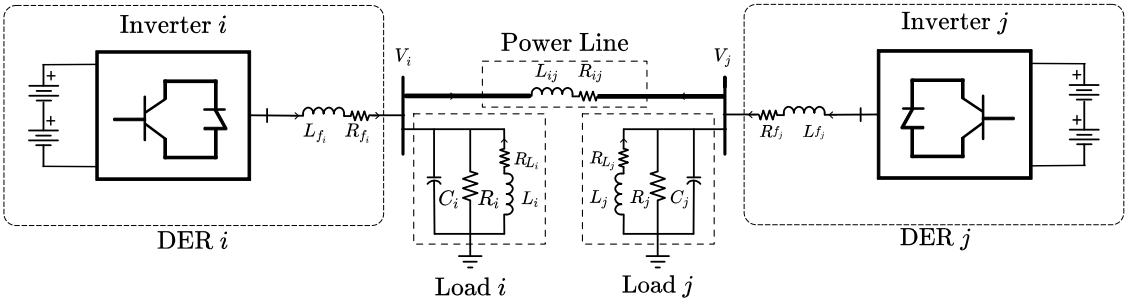

Fig. 1. Schematic of an ImG consisting of two connected subsystems.

The two subsystems are shown in Fig. 1. A nonzero impedance line (R_{ij}, L_{ij}) is connecting the two subsystems. Each subsystem consists of:

- a DER unit consisting of an inverter connecting a DC bus (a stochastic renewable energy sources in series with an energy storage unit) to the PCC through a series filter (R_{f_i} , L_{f_i});
- a parallel three-phase RLC network representing the dedicated load connected at the PCC.

First, the state-space equations of the *i*th subsystem in the *abc*-frame are derived:

$$\begin{aligned}
C_i \frac{dV_{i,abc}}{dt} &= -\frac{V_{i,abc}}{R_i} + I_{i,abc} - I_{L_i,abc} - I_{ij,abc} \\
L_{f_i} \frac{dI_{i,abc}}{dt} &= -V_{i,abc} - R_{f_i} I_{i,abc} + V_{ti,abc} \\
L_i \frac{dI_{L_i,abc}}{dt} &= V_{i,abc} - R_{L_i} I_{L_i,abc} \\
L_{ij} \frac{dI_{ij,abc}}{dt} &= V_{i,abc} - R_{ij} I_{ij,abc} - V_{j,abc}
\end{aligned} \tag{1}$$

The variables in (1) are vectors composed of the three-phase quantities. Under balanced conditions, the application of the dq0 transformation to the state-space equations of (1) in the stationary abc-frame yields to the state-space equations of the *i*th subsystem in a rotating dq-frame with speed ω_0 [17]:

$$\begin{aligned}
C_i \frac{dV_i^{dq}}{dt} + j\omega_0 C_i V_i^{dq} &= -\frac{V_i^{dq}}{R_i} + I_i^{dq} - I_{L_i}^{dq} - I_{ij}^{dq} \\
L_{f_i} \frac{dI_i^{dq}}{dt} + j\omega_0 L_{f_i} I_i^{dq} &= -V_i^{dq} - R_{f_i} I_i^{dq} + V_{t_i}^{dq} \\
L_i \frac{dI_{L_i}^{dq}}{dt} + j\omega_0 L_i I_{L_i}^{dq} &= V_i^{dq} - R_{L_i} I_{L_i}^{dq} \\
L_{ij} \frac{dI_{ij}^{dq}}{dt} + j\omega_0 L_{ij} I_{ij}^{dq} &= V_i^{dq} - R_{ij} I_{ij}^{dq} - V_j^{dq}
\end{aligned} \tag{2}$$

Note that the *i*th and *j*th subsystems are symmetric, therefore, the state-space model of the *j*th subsystem can be obtained by just replacing *i* by *j* in (2), knowing that $R_{ij} = R_{ji}$ and $L_{ij} = L_{ji}$.

Assuming that the initial state $I_{ij}^{dq}(0) = -I_{ji}^{dq}(0)$, it can be concluded that $I_{ij}^{dq}(t) = -I_{ji}^{dq}(t)\ \forall t \geq 0$. This guarantees the definition of two opposite line currents injected by the subsystems. However, since these two line currents represent both the same state, they should not appear in the state-space equations to prevent overlapping state vectors in the overall ImG model. For this purpose, the approximated model of the line in [19] will be used by considering a quasistationary lossless line (quasistationary approximation) and setting $\dot{I}_{ij}^{dq} = \dot{I}_{ji}^{dq} = 0$. Thus, the fourth equation of (2) gives

$$\begin{aligned} I_{ij}^{dq} &= \frac{V_i^{dq} - V_j^{dq}}{R_{ij} + j\omega_0 L_{ij}} \\ &= \frac{R_{ij} - j\omega_0 L_{ij}}{|Z_{ij}|^2} V_i^{dq} - \frac{R_{ij} - j\omega_0 L_{ij}}{|Z_{ij}|^2} V_j^{dq} \end{aligned} \tag{3}$$

where, $Z_{ij} = R_{ij} + j\omega_0 L_{ij}$ and $|Z_{ij}| = \sqrt{R_{ij}^2 + (\omega_0 L_{ij})^2}$.

By replacing I_{ij}^{dq} in (2) with the right-hand side of (3) and removing the fourth equation, the state-space equations become:

$$\begin{aligned} C_i \frac{dV_i^{dq}}{dt} &= \left[-\left(\frac{1}{R_i} + \frac{R_{ij}}{|Z_{ij}|^2} \right) - j\left(\omega_0 C_i - \frac{\omega_0 L_{ij}}{|Z_{ij}|^2} \right) \right] V_i^{dq} + I_i^{dq} - I_{L_i}^{dq} + \frac{R_{ij} - j\omega_0 L_{ij}}{|Z_{ij}|^2} V_j^{dq} \\ L_{f_i} \frac{dI_i^{dq}}{dt} &= -V_i^{dq} - \left(R_{f_i} + j\omega_0 L_{f_i} \right) I_i^{dq} + V_{t_i}^{dq} \\ L_i \frac{dI_{L_i}^{dq}}{dt} &= V_i^{dq} - \left(R_{L_i} + j\omega_0 L_i \right) I_{L_i}^{dq} \end{aligned} \tag{4}$$

Each equation in (4) can be split into two equations, in terms of the real d-axis component and the imaginary q-axis component of the dq-frame, giving

$$\begin{aligned} C_i \frac{dV_i^d}{dt} &= -\left(\frac{1}{R_i} + \frac{R_{ij}}{|Z_{ij}|^2} \right) V_i^d + \left(\omega_0 C_i - \frac{\omega_0 L_{ij}}{|Z_{ij}|^2} \right) V_i^q + I_i^d - I_{L_i}^d + \frac{R_{ij}}{|Z_{ij}|^2} V_j^d + \frac{\omega_0 L_{ij}}{|Z_{ij}|^2} V_j^q \\ C_i \frac{dV_i^q}{dt} &= -\left(\omega_0 C_i - \frac{\omega_0 L_{ij}}{|Z_{ij}|^2} \right) V_i^d - \left(\frac{1}{R_i} + \frac{R_{ij}}{|Z_{ij}|^2} \right) V_i^q + I_i^q - I_{L_i}^q - \frac{\omega_0 L_{ij}}{|Z_{ij}|^2} V_j^d + \frac{R_{ij}}{|Z_{ij}|^2} V_j^q \\ L_{f_i} \frac{dI_i^d}{dt} &= -V_i^d - R_{f_i} I_i^d + \omega_0 L_{f_i} I_i^q + V_{t_i}^d \\ L_{f_i} \frac{dI_i^q}{dt} &= -V_i^q - \omega_0 L_{f_i} I_i^d - R_{f_i} I_i^q + V_{t_i}^q \\ L_i \frac{dI_{L_i}^d}{dt} &= V_i^d - R_{L_i} I_{L_i}^d + \omega_0 L_i I_{L_i}^q \\ L_i \frac{dI_{L_i}^q}{dt} &= V_i^q - \omega_0 L_i I_{L_i}^d - R_{L_i} I_{L_i}^q \end{aligned} \tag{5}$$

It is supposed that the DERs are geographically dispersed; consequently, the lines are mainly inductive $\frac{R_{ij}}{|Z_{ij}|^2} \approx 0$, then

$$
\begin{aligned}
C_i \frac{dV_i^d}{dt} &= -\frac{V_i^d}{R_i} + \left(\omega_0 C_i - \frac{\omega_0 L_{ij}}{|Z_{ij}|^2}\right) V_i^q + I_i^d - I_{L_i}^d + \frac{\omega_0 L_{ij}}{|Z_{ij}|^2} V_j^q \\
C_i \frac{dV_i^q}{dt} &= -\left(\omega_0 C_i - \frac{\omega_0 L_{ij}}{|Z_{ij}|^2}\right) V_i^q - \frac{V_i^q}{R_i} + I_i^q - I_{L_i}^q - \frac{\omega_0 L_{ij}}{|Z_{ij}|^2} V_j^d \\
L_{f_i} \frac{dI_i^d}{dt} &= -V_i^d - R_{f_i} I_i^d + \omega_0 L_{f_i} I_i^q + V_{t_i}^d \\
L_{f_i} \frac{dI_i^q}{dt} &= -V_i^q - \omega_0 L_{f_i} I_i^d - R_{f_i} I_i^q + V_{t_i}^q \\
L_i \frac{dI_{L_i}^d}{dt} &= V_i^d - R_{L_i} I_{L_i}^d + \omega_0 L_i I_{L_i}^q \\
L_i \frac{dI_{L_i}^q}{dt} &= V_i^q - \omega_0 L_i I_{L_i}^d - R_{L_i} I_{L_i}^q
\end{aligned}
\tag{6}
$$

2.2. Model of N interconnected subsystems

Now, the state-space equations of (6) are extended to ImGs with N interconnected subsystems in a meshed topology. In such ImGs, each subsystem $i \in \{1, N\}$ can be connected, through transmission lines, to n_i other subsystems ($1 \le n_i \le N-1$) denoted neighbors of the ith subsystem. Let N_i be the set of these neighbors, the state-space equations of the ith subsystem are given by

$$
\begin{aligned}
C_i \frac{dV_i^d}{dt} &= -\frac{V_i^d}{R_i} + \left(\omega_0 C_i - \sum_{j \in \mathrm{N}_i} \frac{\omega_0 L_{ij}}{|Z_{ij}|^2}\right) V_i^q + I_i^d - I_{L_i}^d + \sum_{j \in \mathrm{N}_i} \frac{\omega_0 L_{ij}}{|Z_{ij}|^2} V_j^q \\
C_i \frac{dV_i^q}{dt} &= -\left(\omega_0 C_i - \sum_{j \in \mathrm{N}_i} \frac{\omega_0 L_{ij}}{|Z_{ij}|^2}\right) V_i^q - \frac{V_i^q}{R_i} + I_i^q - I_{L_i}^q - \sum_{j \in \mathrm{N}_i} \frac{\omega_0 L_{ij}}{|Z_{ij}|^2} V_j^d \\
L_{f_i} \frac{dI_i^d}{dt} &= -V_i^d - R_{f_i} I_i^d + \omega_0 L_{f_i} I_i^q + V_{t_i}^d \\
L_{f_i} \frac{dI_i^q}{dt} &= -V_i^q - \omega_0 L_{f_i} I_i^d - R_{f_i} I_i^q + V_{t_i}^q \\
L_i \frac{dI_{L_i}^d}{dt} &= V_i^d - R_{L_i} I_{L_i}^d + \omega_0 L_i I_{L_i}^q \\
L_i \frac{dI_{L_i}^q}{dt} &= V_i^q - \omega_0 L_i I_{L_i}^d - R_{L_i} I_{L_i}^q
\end{aligned}
\tag{7}
$$

From (7), the descriptor state-space model of the ith subsystem is:

$$
\begin{aligned}
\mathbf{E}_i \dot{x}_i(t) &= \mathbf{A}_{ii} x_i(t) + \mathbf{B}_i u_i(t) + \xi_i(t) \\
y_i(t) &= \mathbf{C}_i x_i(t)
\end{aligned}
\tag{8}
$$

where, $x_i = [V_i^d, V_i^q, I_i^d, I_i^q, I_{L_i}^d, I_{L_i}^q]^T$, $u_i = [V_{t_i}^d, V_{t_i}^q]^T$, and $y_i = [I_i^d, I_i^q]^T$ are the state, the control input, and the controlled output of the *i*th subsystem model, respectively. $\xi_i = \sum_{j \in \mathrm{N}_i} \mathbf{A}_{ij} x_j$ represents the coupling with the neighbors.

Note that the DER current is chosen as the controlled variable instead of the voltage at the PCC; hence, the DERs must track the currents set points. These set points can be dictated by droop control [20] or dynamical optimization [21]. Furthermore, given the fact that the decentralized controllers stabilize their corresponding subsystems, the voltage at the PCC will be regulated and maintained at its nominal value.

The matrices $\mathbf{E}_i$, $\mathbf{A}_{ii}$, $\mathbf{B}_i$, and $\mathbf{C}_i$ are given in the Appendix. It is worth mentioning that $\mathbf{A}_{ij} = -\mathbf{A}_{ji}^T$, $\mathbf{B}_i = \mathbf{C}_i^T$, and $\mathbf{A}_{ii}$ is the sum of a diagonal matrix $\bar{\mathbf{A}}_{ii}$ and a skew-symmetric matrix $\tilde{\mathbf{A}}_{ii}$.

2.3. Model of the Overall Microgrid

The descriptor state-space model of the overall ImG is given by

$$\begin{aligned} \mathbf{E}\dot{x}(t) &= \mathbf{A}x(t) + \mathbf{B}u(t) \\ y(t) &= \mathbf{C}x(t) \end{aligned} \tag{9}$$

where, $x = [x_1, \ldots, x_N]$, $u = [u_1, \ldots, u_N]$ and $y = [y_1, \ldots, y_N]$ are the state, the control input and the controlled output of the overall ImG model, respectively. The matrices $\mathbf{E}$, $\mathbf{B}$ and $\mathbf{C}$ are diagonal matrices such that $\mathbf{E} = diag(\mathbf{E}_1, \ldots, \mathbf{E}_N)$, $\mathbf{B} = diag(\mathbf{B}_1, \ldots, \mathbf{B}_N)$, and $\mathbf{C} = diag(\mathbf{C}_1, \ldots, \mathbf{C}_N)$, while $\mathbf{A}$ is a block matrix that collects the matrices $\mathbf{A}_{ij}$ for all $i,j \in \{1, \ldots, N\}$.

3. Decentralized HSSPFC Design

3.1. Decentralized Control of the subsystems

This section presents the design of the decentralized controllers based on the HSSPFC design procedure. Each controller is designed separately using only information about its corresponding subsystem without requiring any global parameter or any information from other subsystems.

To ensure that the synthesis of the controllers is completely decentralized, the nominal model of the *i*th subsystem is considered by omitting the coupling term $\xi_i(t)$:

$$\mathbf{E}_i \dot{x}_i(t) = \mathbf{A}_{ii} x_i(t) + \mathbf{B}_i u_i(t) \tag{10}$$

Let $\tilde{x}_i$ be the error state defined as follows

$$\tilde{x}_i = x_{i,r} - x_i \tag{11}$$

where, $x_{i,r}$ contains the reference trajectories.

$$\mathbf{E}_i \dot{\tilde{x}}_i(t) = \mathbf{A}_{ii} \tilde{x}_i(t) + \mathbf{B}_i \Delta u_i(t) \tag{12}$$

where, $\Delta u_i = u_{i,r} - u_i$, and $u_{i,r}$ is the feedforward.

Next, the decentralized controller for each subsystem is designed such that the nominal closed-loop subsystem is asymptotically stable. A proportional-integral (PI) controller is chosen to guarantee the regulation of the load voltage at the PCCs and the tracking of the DER's current trajectories by zeroing the steady-state output error $e_i = \mathbf{C}_i \tilde{x}_i$. The PI controller equation is

$$\Delta u_i = -\mathbf{K}_{\mathbf{P}i} \mathbf{B}_i^T \tilde{x}_i - \mathbf{K}_{\mathbf{I}i} \int_0^t e_i d\tau \tag{13}$$

where, $\mathbf{K}_{\mathbf{P}i}$ and $\mathbf{K}_{\mathbf{I}i}$ are the controller gain matrices that will be selected based on the HSSPFC design procedure.

By replacing Δu_i in (12) with the right-hand side of (13), the model of the *i*th nominal closed-loop subsystem is:

$$\begin{bmatrix} \mathbf{E}_i & 0 \\ 0 & \mathbf{K}_{\mathbf{I}i} \end{bmatrix} \begin{bmatrix} \dot{\tilde{x}}_i \\ \dot{\tilde{v}}_i \end{bmatrix} = \begin{bmatrix} \mathbf{A}_{ii} - \mathbf{B}_i \mathbf{K}_{\mathbf{P}i} \mathbf{B}_i^T & -\mathbf{B}_i \mathbf{K}_{\mathbf{I}i} \\ \mathbf{K}_{\mathbf{I}i} \mathbf{C}_i & 0 \end{bmatrix} \begin{bmatrix} \tilde{x}_i \\ \tilde{v}_i \end{bmatrix} \tag{14}$$

where, $\tilde{v}_i = \int_0^t e_i d\tau$, and the augmented state of the *i*th nominal closed-loop subsystem is $\hat{x}_i = \left[\tilde{x}_i, \tilde{v}_i\right]$.

The Hamiltonian of the *i*th nominal closed-loop subsystem is given by

$$\begin{aligned} H_i(\hat{x}_i) &= \frac{1}{2} \hat{x}_i^T \begin{bmatrix} \mathbf{E}_i & 0 \\ 0 & \mathbf{K}_{\mathbf{I}i} \end{bmatrix} \hat{x}_i \\ &= \frac{1}{2} \tilde{x}_i^T \mathbf{E}_i \, \tilde{x}_i + \frac{1}{2} \tilde{v}_i^T \mathbf{K}_{\mathbf{I}i} \tilde{v} \\ &= \frac{1}{2} \tilde{x}_i^T \mathbf{E}_i \, \tilde{x}_i + \frac{1}{2} \left(\int_0^t e_i^T d\tau \right) \mathbf{K}_{\mathbf{I}i} \left(\int_0^t e_i d\tau \right) \end{aligned} \tag{15}$$

since $\mathbf{E}_\mathrm{i}$ is positive definite, a positive definite integral gain $\mathbf{K}_{\mathbf{I}i}$ should be selected to ensure that $H_i(\tilde{x}_i) > 0 \; \forall \hat{x}_i \neq 0$ which is the static stability condition knowing that the Hamiltonian H_i is chosen as a Lyapunov function candidate.

To investigate the asymptotic stability of the *i*th nominal closed-loop subsystem, one must look at the sign of the first-order time derivative of the Hamiltonian:

$$\begin{aligned} \dot{H}_i(\hat{x}_i) &= \tilde{x}_i^T \mathbf{E}_i \dot{\tilde{x}}_i + e_i^T \mathbf{K}_{\mathbf{I}i} \int_0^t e_i d\tau \\ &= \tilde{x}_i^T \left[\left(\mathbf{A}_{ii} - \mathbf{B}_i \mathbf{K}_{\mathbf{P}i} \mathbf{B}_i^T \right) \tilde{x}_i - \mathbf{B}_i \mathbf{K}_{\mathbf{I}i} \int_0^t e_i d\tau \right] + \tilde{x}_i^T \mathbf{C}_i^T \mathbf{K}_{\mathbf{I}i} \int_0^t e_i d\tau \\ &= \tilde{x}_i^T \left(\overline{\mathbf{A}}_{ii} + \tilde{\mathbf{A}}_{ii} \right) \tilde{x}_i - \tilde{x}_i^T \mathbf{B}_i \mathbf{K}_{\mathbf{P}i} \mathbf{B}_i^T \, \tilde{x}_i - \tilde{x}_i^T \mathbf{B}_i \mathbf{K}_{\mathbf{I}i} \int_0^t e_i d\tau + \tilde{x}_i^T \mathbf{C}_i^T \mathbf{K}_{\mathbf{I}i} \int_0^t e_i d\tau \end{aligned} \tag{16}$$

since $\mathbf{B}_i = \mathbf{C}_i^T$ and $\tilde{\mathbf{A}}_{ii}$ is a skew-symmetric matrix $\left(\tilde{x}_i^T \tilde{\mathbf{A}}_{ii} \, \tilde{x}_i = 0 \right)$, the first-order time derivative of the Hamiltonian becomes

$$\dot{H}_i(\hat{x}_i) = -\tilde{x}_i^T \left(\mathbf{B}_i \mathbf{K}_{\mathbf{P}i} \mathbf{B}_i^T - \overline{\mathbf{A}}_{ii} \right) \tilde{x}_i \tag{17}$$

A sufficient condition for the asymptotic stability of the nominal closed-loop subsystem is $\dot{H}_i(\hat{x}_i) < 0$, for all $\hat{x}_i \neq 0$. This implies that $\mathbf{K_{P}}_i$ should be chosen such that $\left(\mathbf{B}_i\mathbf{K_{P}}_i\mathbf{B}_i^T - \bar{\mathbf{A}}_{ii}\right)$ is positive definite. However, the time derivative of the Hamiltonian does not depend on the integrators dynamics. Indeed, $\dot{H}_i(\hat{x}_i) = 0$ for $\tilde{x}_i = 0$, irrespective to the value of $\tilde{v}_i = \int_0^t e_i d\tau$. Consequently, $\dot{H}_i$ is negative semidefinite (i.e. $\dot{H}_i(\hat{x}_i) \leq 0$, for all $\hat{x}_i \neq 0$). The asymptotic stability of the nominal closed-loop subsystem is proven using the following theorem [22].

Theorem 1: *Assume there exists a Lyapunov function V(x) of the dynamical system* $x = f(\dot{x})$. *Let* Ω *be a non-empty set of state vectors such that* $x \in \Omega \Rightarrow \dot{V}(x) = 0.$

If the first k-1 derivatives of V(x), evaluated on the set Ω *, are zero*

$$\frac{d^i V(x)}{dt^i} = 0 \qquad \forall x \in \Omega \qquad i = 1, 2, ..., \mathrm{k}-1$$

and the kth derivative is negative definite on the set Ω

$$\frac{d^k V(x)}{dt^k} < 0 \qquad \forall x \in \Omega$$

then the system x(t) is asymptotically stable if k is an odd number.

Using **Theorem 1**, the higher order time derivatives of the Hamiltonian are investigated to prove asymptotic stability. From equation (17), $\Omega_i = \{\hat{x}_i = (\tilde{x}_i, \int_0^t e_i) \mid \tilde{x} = 0\}$.

The first order time derivate of the Hamiltonian is

$$\dot{H}_i(\hat{x}_i) = 0 \quad \forall \hat{x}_i \in \Omega_i. \tag{18}$$

The second order time derivate of the Hamiltonian is

$$\begin{aligned} \ddot{H}_i(\hat{x}_i) &= -2\,\tilde{x}_i^T\left(\mathbf{B}_i\mathbf{K_{P}}_i\mathbf{B}_i^T - \bar{\mathbf{A}}_{ii}\right)\dot{\tilde{x}}_i \\ &= -2\tilde{x}_i^T(\mathbf{B}_i\mathbf{K_{P}}_i\mathbf{B}_i^T - \bar{\mathbf{A}}_{ii})\mathbf{E}_i^{-1}\left[(\mathbf{A}_{ii} - \mathbf{B}_i\mathbf{K_{P}}_i\mathbf{B}_i^T)\tilde{x}_i - \mathbf{B}_i\mathbf{K_{I}}_i\mathbf{C}_i\int_0^t \tilde{x}_i d\tau\right] \\ &= 0 \quad \forall \hat{x}_i \in \Omega_i \end{aligned} \tag{19}$$

The third order time derivate of the Hamiltonian is

$$\begin{aligned} \dddot{H}_i(\hat{x}_i) &= -2\dot{\tilde{x}}_i^T\left(\mathbf{B}_i\mathbf{K_{P}}_i\mathbf{B}_i^T - \bar{\mathbf{A}}_{ii}\right)\mathbf{E}_i^{-1}\left[\left(\mathbf{A}_{ii} - \mathbf{B}_i\mathbf{K_{P}}_i\mathbf{B}_i^T\right)\tilde{x}_i - \mathbf{B}_i\mathbf{K_{I}}_i\int_0^t e_i d\tau\right] - 2\tilde{x}_i^T(\mathbf{B}_i\mathbf{K_{P}}_i\mathbf{B}_i^T - \bar{\mathbf{A}}_{ii})\mathbf{E}_i^{-1}\left[(\mathbf{A}_{ii}\right. \\ &\quad \left. - \mathbf{B}_i\mathbf{K_{P}}_i\mathbf{B}_i^T)\dot{\tilde{x}}_i - \mathbf{B}_i\mathbf{K_{I}}_i\mathbf{C}_i\tilde{x}_i\right] \\ &= -2\left[\mathbf{E}_i^{-1}\left[\left(\mathbf{A}_{ii} - \mathbf{B}_i\mathbf{K_{P}}_i\mathbf{B}_i^T\right)\tilde{x}_i - \mathbf{B}_i\mathbf{K_{I}}_i\int_0^t e_i d\tau\right]\right]^T\left(\mathbf{B}_i\mathbf{K_{P}}_i\mathbf{B}_i^T - \bar{\mathbf{A}}_{ii}\right)\mathbf{E}_i^{-1}\left[\left(\mathbf{A}_{ii} - \mathbf{B}_i\mathbf{K_{P}}_i\mathbf{B}_i^T\right)\tilde{x}_i - \mathbf{B}_i\mathbf{K_{I}}_i\int_0^t e_i d\tau\right] \\ &\quad - 2\tilde{x}_i^T\left(\mathbf{B}_i\mathbf{K_{P}}_i\mathbf{B}_i^T - \bar{\mathbf{A}}_{ii}\right)\mathbf{E}_i^{-1}\left[\left(\mathbf{A}_{ii} - \mathbf{B}_i\mathbf{K_{P}}_i\mathbf{B}_i^T\right)\mathbf{E}_i^{-1}\left[\left(\mathbf{A}_{ii} - \mathbf{B}_i\mathbf{K_{P}}_i\mathbf{B}_i^T\right)\tilde{x}_i - \mathbf{B}_i\mathbf{K_{I}}_i\int_0^t e_i d\tau\right] - \mathbf{B}_i\mathbf{K_{I}}_i\mathbf{C}_i\tilde{x}_i\right] \\ &= -2\left[\mathbf{E}_i^{-1}\mathbf{B}_i\mathbf{K_{I}}_i\int_0^t e_i d\tau\right]^T\left(\mathbf{B}_i\mathbf{K_{P}}_i\mathbf{B}_i^T - \bar{\mathbf{A}}_{ii}\right)\left[\mathbf{E}_i^{-1}\mathbf{B}_i\mathbf{K_{I}}_i\int_0^t e_i d\tau\right] < 0 \quad \forall \hat{x}_i \in \Omega_i. \end{aligned} \tag{20}$$

The order of the first non-zero time derivative of the Hamiltonian H_i is an odd number. Therefore, the ith nominal closed-loop subsystem is asymptotically stable.

3.2. Decentralized Control of the meshed ImG

In this Section, the effect of the decentralized controllers on the stability of the overall closed-loop ImG is investigated. The Hamiltonian of the overall closed-loop ImG is

$$H = \frac{1}{2}\tilde{x}^T \mathbf{E}\,\tilde{x} + \frac{1}{2}\left(\int_0^t e^T d\tau\right)\mathbf{K_I}\left(\int_0^t e d\tau\right) \tag{21}$$

where, $\tilde{x} = [\tilde{x}_1,\ldots,\tilde{x}_N]$ and $e = [e_1,\ldots,e_N]$ are the state error and the output error of the overall closed-loop ImG, respectively, and $\mathbf{K_I} = diag(\mathbf{K_{I1}},\ldots,\mathbf{K_{IN}})$.

The Hamiltonian H of the overall closed-loop ImG is positive define ($\mathbf{E}$ and $\mathbf{K_I}$ are positive definite) and the overall ImG is statically stable.

The time derivative of the Hamiltonian is

$$\begin{aligned}
\dot{H}(\hat{x}) &= \tilde{x}^T \mathbf{E}\dot{\tilde{x}} + e^T \mathbf{K_I}\int_0^t e d\tau \\
&= \tilde{x}^T(\mathbf{E}\dot{x}_r - \mathbf{E}\dot{x}) + e^T \mathbf{K_I}\int_0^t e d\tau \\
&= \tilde{x}^T(\mathbf{A}x_r + \mathbf{B}u_r - \mathbf{A}x - \mathbf{B}u) + e^T \mathbf{K_I}\int_0^t e d\tau \\
&= \tilde{x}^T\mathbf{A}\,\tilde{x} + \tilde{x}^T\mathbf{B}(u_{i,r} - u) + e^T \mathbf{K_I}\int_0^t e d\tau \\
&= \tilde{x}^T\mathbf{A}\,\tilde{x} + \tilde{x}^T\mathbf{B}\Delta u + \tilde{x}^T\mathbf{B}\mathbf{K_I}\int_0^t e d\tau
\end{aligned} \tag{22}$$

where, $\Delta u = (\Delta u_1,\ldots,\Delta u_N)$. Then,

$$\Delta u = -\mathbf{K_P}\mathbf{B}^T\tilde{x} - \mathbf{K_I}\int_0^t e d\tau \tag{23}$$

where, $\mathbf{K_P} = diag(\mathbf{K_{P1}},\ldots,\mathbf{K_{PN}})$. Since, for all $i \in \{1,\ldots,N\}$, $\mathbf{A}_{ij} = -\mathbf{A}_{ji}^T$ and $\mathbf{A}_{ii} = \tilde{\mathbf{A}}_{ii} + \overline{\mathbf{A}}_{ii}$, $\mathbf{A}$ can be written as the sum of a diagonal matrix $\overline{\mathbf{A}} = diag(\overline{\mathbf{A}}_{ii})$ and a skew-symmetric matrix $\tilde{\mathbf{A}} = \mathbf{A} - \overline{\mathbf{A}}$. Then

$$\begin{aligned}
\dot{H}(\hat{x}) &= \tilde{x}^T\overline{\mathbf{A}}\,\tilde{x} - \tilde{x}^T\mathbf{B}\mathbf{K_P}\mathbf{B}^T\tilde{x} - \tilde{x}^T\mathbf{B}\mathbf{K_I}\int_0^t e d\tau + \tilde{x}^T\mathbf{B}\mathbf{K_I}\int_0^t e d\tau \\
&= -\tilde{x}^T(\mathbf{B}\mathbf{K_P}\mathbf{B}^T - \overline{\mathbf{A}})\tilde{x} \\
&= \sum_{i=1}^{N}\left[-\tilde{x}_i^T\left(\mathbf{B}_i\mathbf{K_{P}}_i\mathbf{B}_i^T - \overline{\mathbf{A}}_{ii}\right)\tilde{x}_i\right] \\
&= \sum_{i=1}^{N}\dot{H}_i \le 0, \quad \forall \hat{x} \ne 0
\end{aligned} \tag{24}$$

For asymptotic stability of the overall closed-loop ImG, the time derivative of the Hamiltonian H must be negative definite. Since its negative semi-definite, one should explore the higher order time derivatives of the Hamiltonian.

It goes without saying that $\Omega = \Omega_1 \times \ldots \times \Omega_N$ is the set such that $\dot{H}(\hat{x}) = 0$ for all $\hat{x} \in \Omega$. Thus, the second order derivative of the Hamiltonian is

$$\begin{aligned} \ddot{H} &= \sum_{i=1}^{N} \ddot{H}_i \\ &= 0 \quad \forall \hat{x} \in \Omega. \end{aligned} \tag{25}$$

The third order derivative of the Hamiltonian is

$$\dddot{H} = \sum_{i=1}^{N} \dddot{H}_i < 0 \quad \forall \hat{x} \in \Omega. \tag{26}$$

Therefore, the overall closed-loop ImG is asymptotically stable. This proves the ability of the decentralized controllers to stabilize overall ImG.

4. Performance Evaluation

In this section, the performance of the decentralized Hamiltonian control proposed in this paper is evaluated. The ImG of Fig. 1 was modeled and simulated in Matlab/Simulink. This simulation assesses the performance of the designed controllers regarding the voltage regulation at the PCCs and the DER's reference current tracking. The parameters values used in this simulation are similar to those of reference [23].

In this simulation, the dq components of the load voltage at PCC1 are regulated at 0.8 and 0.7 per-unit (p.u.) and those of PCC2 are regulated at 0.3 and 0.2 p.u., respectively. While the d and q components of the DER1 current set point are stepped up from 0.6 to 0.7 p.u. at t = 0.5 s and from 0.4 to 0.3 p.u. at t = 0.7s, respectively, the d and q components of the DER2 current set point are stepped up from 0.8 to 0.7 p.u. at t = 0.6s and from 0.4 to 0.5 p.u. at t = 0.8 s, respectively.

Fig. 2 and Fig. 3 depict the dynamic responses of the ImG. In particular, Fig. 2(a) and Fig. 2(b) show the d and q components of the PCC1 and PCC2 voltages, respectively. The instantaneous three-phase voltages of PCC1 and PCC2 in the abc-frame are shown in Fig. 2(c) and Fig. 2(d), respectively. It is observed that the decentralized controllers succeed in maintaining and regulating the load voltages at PCC1 and PCC2.

The d and q components of the DER1 and DER2 currents are depicted in Fig. 3(a) and Fig. 3(b), respectively. Fig. 3(c) and Fig. 3(d) present the instantaneous three-phase currents of DER1 and DER2 in the abc-frame, respectively. It can be seen that the proposed decentralized control strategy ensures a fast tracking of the current set points.

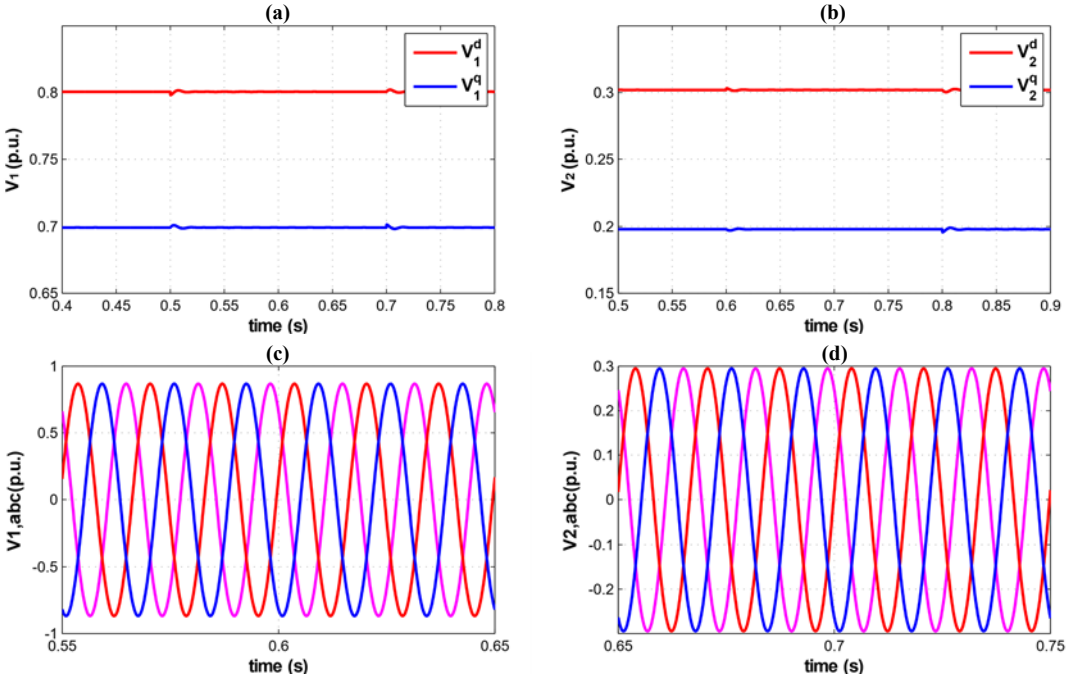

Fig. 2 Performance of the decentralized Hamiltonian control: (a,b) dq components of load voltage at PCC1 and PCC2, (c,d) Instantaneous three-phase voltage at PCC1 and PCC2.

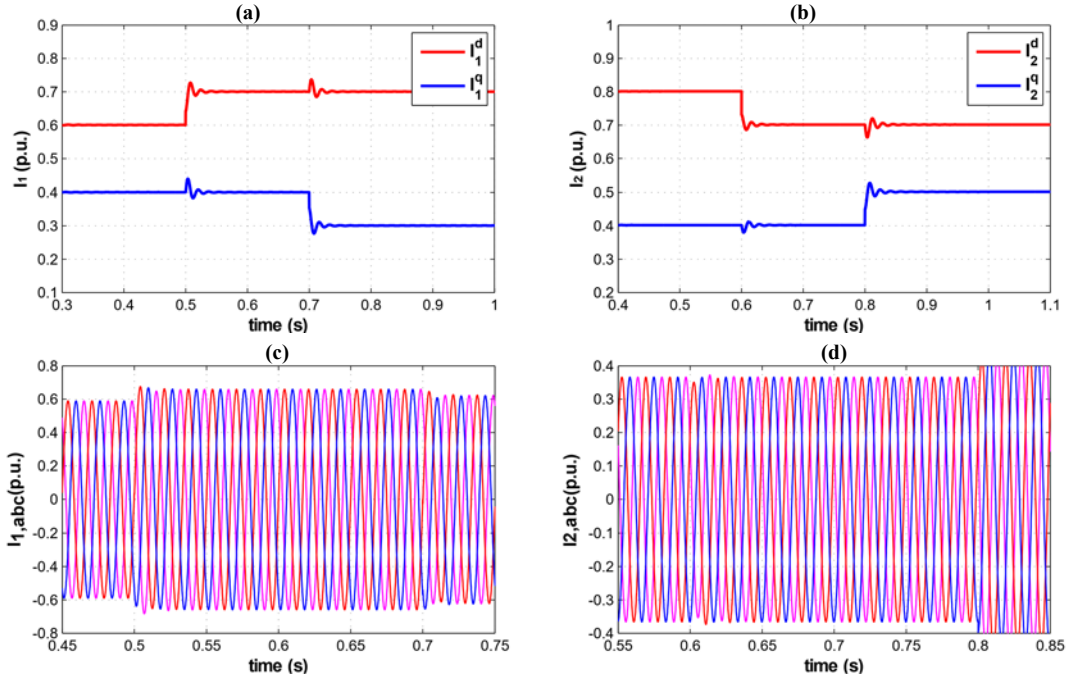

Fig. 3 Performance of the decentralized Hamiltonian control: (a,b) dq components of the currents of DER1 and DER2, (c,d) Instantaneous three-phase currents of DER1 and DER2.

5. Conclusion

In this paper, a model of ImGs with meshed topology was developed. Then, using the HSSPFC design procedure, the decentralized controllers are designed to regulate the voltage at the PCCs, track the DER's current set trajectories, and ensure the stabilization of the overall ImG. The design procedure presented is fully decentralized since it only uses local information to design the controllers, allowing PnP operations for the ImG and guarantying its scalability. Simulation results demonstrated that the proposed designed decentralized controllers can guarantee the regulation of the voltage at the PCCs and the tracking of the DER's current set points. Future work will incorporate robustness against model deviation and improve performance and disturbance rejection.

Acknowledgments

This work was supported in part by the US National Science Foundation (Grant #1541148), the Richard and Elizabeth Henes Professorship of Mechanical Engineering at Michigan Technological University, and the Institute for Research on Solar and new Energies (IRESEN) in Morocco (reference: InnoTherm-13- MicroCSP).

Appendix

$$\mathbf{A}_{ii}=\begin{bmatrix} \frac{-1}{R_i} & \omega_0 C_i-\sum_{j\in\mathcal{N}_i}\frac{\omega_0 L_{ij}}{|Z_{ij}|^2} & 1 & 0 & -1 & 0 \\ -\omega_0 C_i+\sum_{j\in\mathcal{N}_i}\frac{\omega_0 L_{ij}}{|Z_{ij}|^2} & \frac{-1}{R_i} & 0 & 1 & 0 & -1 \\ -1 & 0 & -R_{f_i} & \omega_0 L_{f_i} & 0 & 0 \\ 0 & -1 & -\omega_0 L_{f_i} & -R_{f_i} & 0 & 0 \\ 1 & 0 & 0 & 0 & -R_{L_i} & \omega_0 L_i \\ 0 & 1 & 0 & 0 & -\omega_0 L_i & -R_{L_i} \end{bmatrix}$$

$$\mathbf{A}_{ij}=\begin{bmatrix} 0 & \sum_{j\in\mathcal{N}_i}\frac{\omega_0 L_{ij}}{|Z_{ij}|^2} & 0 & 0 & 0 & 0 \\ -\sum_{j\in\mathcal{N}_i}\frac{\omega_0 L_{ij}}{|Z_{ij}|^2} & 0 & 0 & 0 & 0 & 0 \\ 0 & 0 & 0 & 0 & 0 & 0 \\ 0 & 0 & 0 & 0 & 0 & 0 \\ 0 & 0 & 0 & 0 & 0 & 0 \\ 0 & 0 & 0 & 0 & 0 & 0 \end{bmatrix}=-\mathbf{A}_{ji}^T \qquad \mathbf{E}_i=\begin{bmatrix} C_i & 0 & 0 & 0 & 0 & 0 \\ 0 & C_i & 0 & 0 & 0 & 0 \\ 0 & 0 & L_{f_i} & 0 & 0 & 0 \\ 0 & 0 & 0 & L_{f_i} & 0 & 0 \\ 0 & 0 & 0 & 0 & L_i & 0 \\ 0 & 0 & 0 & 0 & 0 & L_i \end{bmatrix}$$

$$\mathbf{B}_i=\begin{bmatrix} 0 & 0 \\ 0 & 0 \\ 1 & 0 \\ 0 & 1 \\ 0 & 0 \\ 0 & 0 \end{bmatrix} \qquad \mathbf{C}_i=\begin{bmatrix} 0 & 0 & 1 & 0 & 0 & 0 \\ 0 & 0 & 0 & 1 & 0 & 0 \end{bmatrix}$$

References

[1] Bidram A, Davoudi A. Hierarchical Structure of Microgrids Control System. IEEE Transactions on Smart Grid 2012;3:1963–76. doi:10.1109/TSG.2012.2197425.
[2] Yang N, Paire D, Gao F, Miraoui A. Power management strategies for microgrid-A short review. Industry Applications Society Annual Meeting, 2013 IEEE, IEEE; 2013, p. 1–9.
[3] Martins AP, Carvalho AS, Araujo AS. Design and implementation of a current controller for the parallel operation of standard UPSs. , Proceedings of the 1995 IEEE IECON 21st International Conference on Industrial Electronics, Control, and Instrumentation, 1995, vol. 1, 1995, p. 584–9 vol.1. doi:10.1109/IECON.1995.483474.
[4] Tenti P, Caldognetto T, Costabeber A, Mattavelli P. Microgrids operation based on master-slave cooperative control. IECON 2013 - 39th Annual Conference of the IEEE Industrial Electronics Society, 2013, p. 7623–8. doi:10.1109/IECON.2013.6700403.
[5] Sun X, Lee Y-S, Xu D. Modeling, analysis, and implementation of parallel multi-inverter systems with instantaneous average-current-sharing scheme. IEEE Transactions on Power Electronics 2003;18:844–56. doi:10.1109/TPEL.2003.810867.
[6] Chandorkar MC, Divan DM, Adapa R. Control of parallel connected inverters in standalone AC supply systems. IEEE Transactions on Industry Applications 1993;29:136–43. doi:10.1109/28.195899.
[7] Karimi H, Davison EJ, Iravani R. Multivariable Servomechanism Controller for Autonomous Operation of a Distributed Generation Unit: Design and Performance Evaluation. IEEE Transactions on Power Systems 2010;25:853–65.
[8] Etemadi AH, Davison EJ, Iravani R. A Decentralized Robust Control Strategy for Multi-DER Microgrids—Part I: Fundamental Concepts. IEEE Transactions on Power Delivery 2012;27:1843–53.
[9] Rocabert J, Luna A, Blaabjerg F, Rodríguez P. Control of Power Converters in AC Microgrids. IEEE Transactions on Power Electronics 2012;27:4734–49.
[10] Etemadi AH, Davison EJ, Iravani R. A Generalized Decentralized Robust Control of Islanded Microgrids. IEEE Transactions on Power Systems 2014;29:3102–13.
[11] Guerrero JM, Chandorkar M, Lee TL, Loh PC. Advanced Control Architectures for Intelligent Microgrids x2014;Part I: Decentralized and Hierarchical Control. IEEE Transactions on Industrial Electronics 2013;60:1254–62. doi:10.1109/TIE.2012.2194969.
[12] Riverso S, Sarzo F, Ferrari-Trecate G. Plug-and-Play Voltage and Frequency Control of Islanded Microgrids With Meshed Topology. IEEE Transactions on Smart Grid 2015;6:1176–84. doi:10.1109/TSG.2014.2381093.
[13] Toub M, Aniba G, Maaroufi M, Robinet RD. Decentralized Hamiltonian control of isolated AC microgrids: Theory amp; design. Smart Grid Technologies - Asia (ISGT ASIA), 2015 IEEE Innovative, 2015, p. 1–6. doi:10.1109/ISGT-Asia.2015.7387194.
[14] Wilson DG, Robinett RD. Transient stability and performance based on nonlinear power flow control design of renewable energy systems. 2011 IEEE International Conference on Control Applications (CCA), 2011, p. 881–6. doi:10.1109/CCA.2011.6044370.
[15] Wilson DG, Neely JC, Cook MA, Glover SF, Young J, Robinett RD. Hamiltonian control design for DC microgrids with stochastic sources and loads with applications. Power Electronics, Electrical Drives, Automation and Motion (SPEEDAM), 2014 International Symposium on, 2014, p. 1264–71. doi:10.1109/SPEEDAM.2014.6872094.
[16] Robinett RD, Wilson DG. Nonlinear power flow control design for combined conventional and variable generation systems: Part I-theory. 2011 IEEE International Conference on Control Applications (CCA), 2011, p. 61–4. doi:10.1109/CCA.2011.6044377.
[17] Hassell T, Weaver WW, Robinett RD, Wilson DG, Parker GG. Modeling of inverter based Ac microgrids for control development. 2015 IEEE Conference on Control Applications (CCA), 2015, p. 1347–53. doi:10.1109/CCA.2015.7320799.
[18] Robinett III RD, Wilson DG. Nonlinear power flow control design: utilizing exergy, entropy, static and dynamic stability, and Lyapunov analysis. Springer Science & Business Media; 2011.
[19] Venkatasubramanian V, Schattler H, Zaborszky J. Fast time-varying phasor analysis in the balanced three-phase large electric power system. IEEE Transactions on Automatic Control 1995;40:1975–82. doi:10.1109/9.471228.
[20] Toub M, Weaver WW, Robinett RD, Maaroufi M, Aniba G. A DQ droop control strategy for fixed frequency VSI-based AC microgrids. 2018 5th International Conference on Renewable Energy: Generation and Applications (ICREGA), 2018, p. 332–5. doi:10.1109/ICREGA.2018.8337641.
[21] Parker GG, Weaver WW, Robinett RD, Wilson DG. Optimal DC microgrid power apportionment and closed loop storage control to mitigate source and load transients. Resilience Week (RWS), 2015, 2015, p. 1–7. doi:10.1109/RWEEK.2015.7287420.
[22] Schaub H, Junkins JL. Analytical Mechanics of Space Systems. 3rd ed. Reston, VA: AIAA Education Series; 2014. doi:10.2514/4.102400.
[23] Moradi R, Karimi H, Karimi-Ghartemani M. Robust decentralized control for islanded operation of two radially connected DG systems. 2010 IEEE International Symposium on Industrial Electronics, 2010, p. 2272–7. doi:10.1109/ISIE.2010.5637651.